Plastic/Ferroelectric Crystals with Distorted Molecular Arrangement: Ferroelectricity in Bulk Polycrystalline Films through Lattice Reorientation

Jun Harada, Mika Takehisa, Yuto Kawamura, Haruka Takahashi, and Yukihiro Takahashi*

Dr. J. Harada, M. Takehisa, Dr. Y. Takahashi
Department of Chemistry, Faculty of Science, Hokkaido University
Kita 10, Nishi 8 Kita-ku, Sapporo Hokkaido, 060-0810, Japan
E-mail: junharada@sci.hokudai.ac.jp

Dr. J. Harada, Y. Kawamura, H. Takahashi, Dr. Y. Takahashi
Graduate School of Chemical Sciences and Engineering, Hokkaido University
Kita 10, Nishi 8 Kita-ku, Sapporo Hokkaido, 060-0810, Japan

Keywords: ferroelectrics, plastic crystals, molecular crystals, crystal structures, bulk materials

Abstract: Plastic/ferroelectric crystals have attracted increasing attention as emerging functional molecular materials with unique features. In this study, a new plastic/ferroelectric crystal has been developed from ionic molecules, which exhibits three solid phases: a paraelectric plastic crystal phase and two ferroelectric phases. Owing to the malleability in the plastic crystal phase, by applying pressure to the powder at a high temperature, transparent polycrystalline films are easily fabricated, exhibiting ferroelectric performance at room temperature. The crystal structures of the three solid phases have been determined by single-crystal X-ray diffraction analysis. The arrangement of anions and cations in the ferroelectric crystal is significantly distorted from the CsCl-type structure in the paraelectric cubic crystal. The large distortion results in distinct splitting of the diffraction peaks that are equivalent in the cubic phase, which enables the observation of electric-field-induced lattice reorientation using powder X-ray diffraction measurements. These results broaden the range of compounds for which plastic/ferroelectric crystals can be developed and provide a solid understanding of the switching process in their bulk polycrystals, which will facilitate their application to a variety of device elements.

1. Introduction

Plastic crystals have recently attracted growing interest as molecular materials that exhibit a variety of functions.[1] Plastic crystals are a class of molecular compounds that have a

mesophase, that is, a plastic crystal phase between the solid and liquid phases.[2] In the plastic crystal phase, the constituent molecules maintain their three-dimensional positional order, forming a crystal lattice similar to that of an ordinary crystal. In contrast, the molecular orientation is completely disordered, as in a liquid, owing to the rapid isotropic rotations of the molecules. Plastic crystals consist of molecules with globular structures, such as adamantane, which has a nearly spherical shape, and tetrabromomethane, with a tetrahedral shape. Such globular molecules can easily rotate in crystals. Plastic crystals exhibit plastic deformation (malleability) without a fracture like waxes upon application of uniaxial pressure. Moreover, they exhibit several unique features that are different from ordinary molecular crystals, such as self-diffusion of molecules and large entropy changes in solid-solid phase transitions. These characteristics have been exploited for the development of functional materials with high ion conductivity and colossal barocaloric effects, respectively.[3,4]

Plastic/ferroelectric crystals are another class of functional materials that have a plastic crystal phase as a paraelectric phase at high temperatures and a ferroelectric phase at low temperatures.[5] Owing to the cubic crystal symmetry in the paraelectric phase, which is another unique feature of plastic crystals, plastic/ferroelectric crystals exhibit multiaxial ferroelectricity. In contrast to the uniaxial ferroelectricity of conventional molecular ferroelectric crystals, the multiaxial ferroelectricity of plastic/ferroelectric crystals enables ferroelectric performance in bulk polycrystalline forms for the first time as molecular ferroelectric crystals.[6] Therefore, plastic/ferroelectric crystals have solved the problem of the low dimensionality of molecular ferroelectric crystals, where the ferroelectric performance is limited to single crystals with suitable orientations and shapes. Some of the plastic/ferroelectric crystals show large piezoelectricity and pyroelectricity in their bulk polycrystalline forms.[7,8]

Although a considerable number of plastic/ferroelectric crystals and related ferroelectric crystals have been reported to exhibit multiaxial ferroelectricity, their ferroelectric performance in bulk polycrystals is rather limited.[5-9] This is partly due to the large coercive field (E_c) values

of such ferroelectric crystals. Some of the plastic/ferroelectric crystals have small E_c values at room temperature, typically less than 5 kV cm^{-1}, and low-voltage performance,[8] whereas others have E_c values larger than 100 kV cm^{-1}. The application of such ferroelectric crystals with large E_c values is limited to thin crystalline films grown on substrates.

To use plastic/ferroelectric crystals as bulk materials for a wide range of applications, it is necessary to develop plastic/ferroelectric crystals from molecules with various shapes and to investigate the relationship between molecular/crystal structures and physical properties such as E_c values. In this study, we developed a new plastic/ferroelectric crystal, 1-methyl-4-aza-1-azoniabicyclo[2.2.2]octanium hexafluorophosphate [MDABCO][PF_6] (**1**). The [MDABCO]$^+$ cation is a derivative of 1,4-diazabicyclo[2.2.2]octane (DABCO) and has a structure consisting of a sphere (DABCO) with a protrusion (methyl group). The ionic molecule has a dipole moment parallel to the three-fold axis of the molecule. While the combination of the monoprotonated cation of DABCO ([HDABCO]$^+$) and tetrahedral anions such as BF_4^-, ClO_4^-, and ReO_4^- forms plastic/ferroelectric crystals,[9a,10] plastic/ferroelectric crystals containing the [MDABCO]$^+$ cation or the $[PF_6]^-$ anion have not been reported yet. Crystal **1** has a plastic crystal phase above 327 K and two ferroelectric phases at lower temperatures. The arrangement of cations and anions in the ferroelectric phases was largely distorted from that in the paraelectric phase, and the bulk polycrystalline films showed ferroelectricity with large E_c values. We also observed lattice reorientation induced by electric fields using powder X-ray diffraction (XRD) measurements, which is unprecedented for multiaxial molecular ferroelectric crystals.

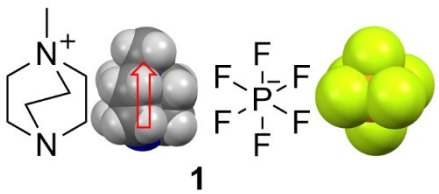

1

2. Results and Discussion

2.1. Phase Transitions

Differential scanning calorimetry (DSC) measurements of the crystals of **1** revealed two solid-solid phase transitions: one below and the other above room temperature (at 246 K and 327 K in the heating runs, respectively) **(Figure 1)**. Hereafter, we will refer to the three solid phases separated by the two transitions as the low-temperature phase (LTP), room-temperature phase (RTP), and high-temperature phase (HTP). The large entropy change observed at the RTP/HTP transition (12.2 J K^{-1} mol^{-1}) is characteristic of the transition from an ordinary crystal phase to a plastic crystal phase, which involves a large increase in degrees of freedom in molecular orientation.

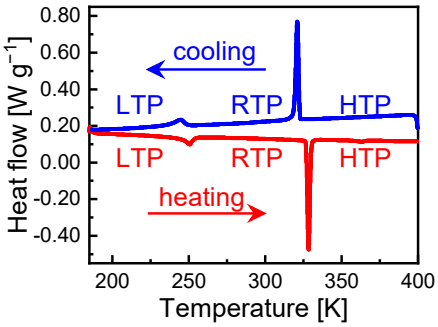

Figure 1. DSC traces of [MDABCO][PF_6] (**1**), where the solid phases are labelled as LTP, RTP, and HTP.

2.2. Crystal Structures

The crystal structures of **1** in the three phases were determined by single-crystal XRD analyses, which were consistent with plastic/ferroelectric crystals **(Figure 2)**. The crystal and experimental data are listed in Table 1. In the HTP at 350 K, the crystal belongs to the cubic crystal system, and the space group is assigned as $Pm\bar{3}m$. The orientation of the $[MDABCO]^+$ cations is completely disordered, as is often observed for molecules in plastic crystals (Figure 2a). The large atomic displacement parameters of the $[PF_6]^-$ anions also indicate the orientational motions of the ionic molecules. Although only limited structural information is available from the crystal structure of the HTP, the CsCl-type cubic structures of rotating ionic molecules are consistent with the plastic crystal phase.

The crystal structure of **1** in the RTP at 300 K belongs to the orthorhombic crystal system (Figure 2b). The polar point group *mm*2 and space group $Pmc2_1$ are consistent with a ferroelectric phase, where the spontaneous polarization is parallel to the *c*-axis. The $[MDABCO]^+$ cations take two different orientations resulting in orientational disorder, whereas the dipole moment is oriented in one direction at each site. Although the cations and anions maintain the eight-coordinated arrangement as that in the HTP, the arrangement in the RTP is highly distorted from the cubic arrangement in the HTP, and the eight $[PF_6]^-$ anions surrounding the $[MDABCO]^+$ cation form a right prism with a kite base (Figure 2c). Compared to the cube with a side of 6.61 Å in the HTP, the different lengths of the three sides in the right prism, that is, 5.83, 7.41, and 6.47 Å (the length of the *a*-axis), indicate a large distortion of the molecular arrangement in the ferroelectric phase. The large distortion from the cubic structure in the RTP of **1** makes a sharp contrast to small distortions in the rhombohedral lattices in some of the plastic/ferroelectric crystals exhibiting ferroelectric polarization switching in bulk polycrystals with small E_c values.[6,8] The largely distorted molecular arrangement in the RTP of **1** arises from the shape of the $[MDABCO]^+$ cation, which has a protruding methyl group and deviates from the spherical shape. The molecular arrangement in the RTP implies that ferroelectric polarization switching requires the application of large electric fields. Moreover, the crystal might not show a multiaxial ferroelectric switching involving substantial repositioning of all $[PF_6]^-$ anions, rather a uniaxial ferroelectric switching between the two orientations (Figure 2c and d) through a flip-flop motion of the cation without substantial repositioning of the anions.

The crystal structure in the LTP (at 180 K) also belongs to the polar point group *mm*2 (orthorhombic crystal system, space group: $Pca2_1$) **(Figure S1)**. Although the overall arrangement of the cations and anions is similar to that in the RTP, that is, a distorted CsCl-type structure, no orientational disorder was detected for either the cation or anion. Although the polar crystal structure in the LTP is consistent with a ferroelectric phase, ferroelectric switching is expected to involve large coercive fields.

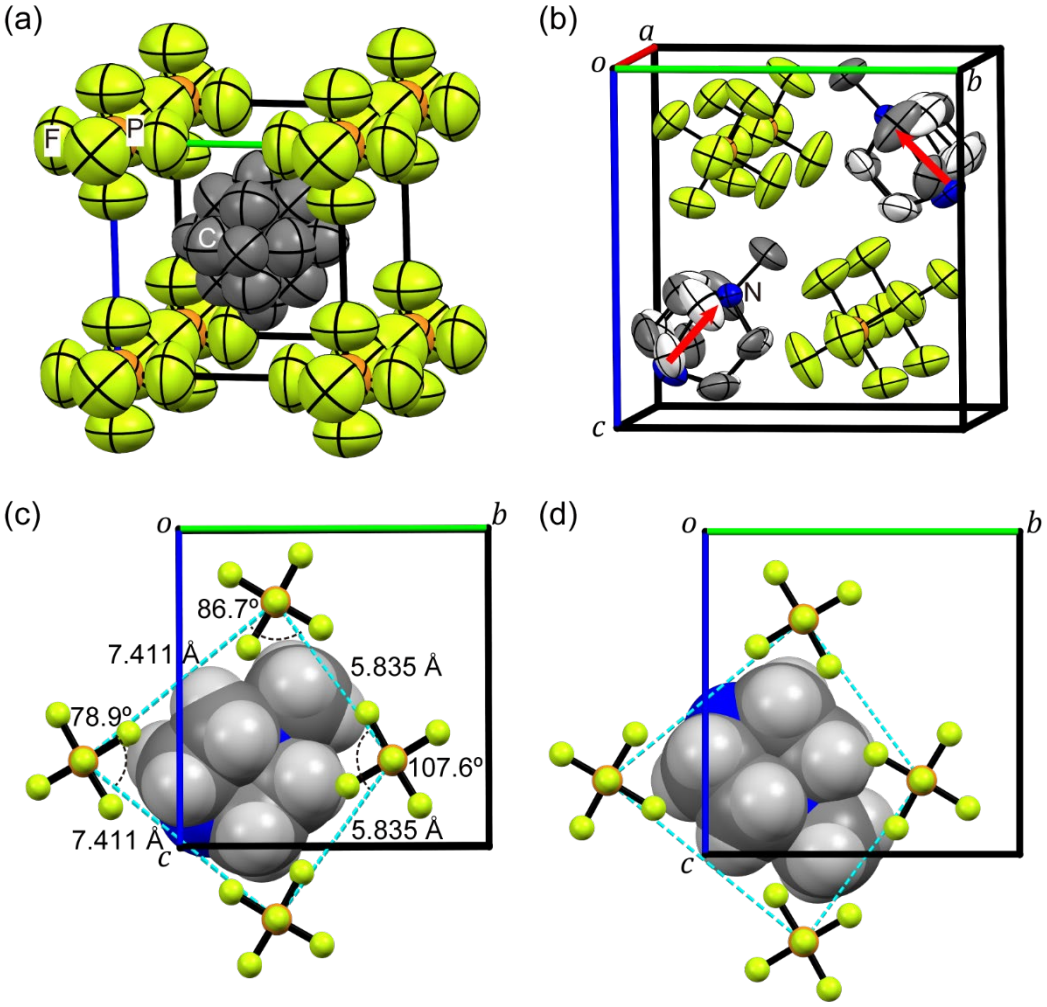

Figure 2. Crystal structures of [MDABCO][PF_6] (**1**). Thermal ellipsoids in (a) and (b) are drawn at 50% probability. (a) At 350 K (HTP). (b) At 300 K (RTP). Hydrogen atoms are omitted for clarity. The carbon atoms of one of the two disordered orientations of $[MDABCO]^+$ cations are depicted in white. The direction of the dipole moment of each $[MDABCO]^+$ cation is indicated by a red arrow. (c) Projection along the *a*-axis at 300 K (RTP), where the distorted CsCl-type arrangement is outlined by dashed cyan lines connecting phosphor atoms of the $[PF_6]^-$ anions. Only one of the two orientations of $[MDABCO]^+$ cation is displayed. (d) Projection along *a*-axis at 300 K (RTP) generated by inverting the experimentally obtained structure shown in (c).

Table 1. Crystal Data and Structure Refinement Information for **1**

Compound		[MDABCO][PF_6] (**1**)	
Temperature [K]	350	300	180

Phase	HTP	RTP	LTP
Empirical formula		$C_7H_{15}N_2F_6P$	
Formula weight		272.18	
Crystal system	Cubic	Orthorhombic	Orthorhombic
Space group	$Pm\bar{3}m$	$Pmc2_1$	$Pca2_1$
a [Å]	6.6085(14)	6.4684(7)	17.7703(11)
b [Å]	6.6085(14)	9.1684(9)	6.2751(4)
c [Å]	6.6085(14)	9.4186(10)	9.5724(6)
V [Å^3]	288.61(18)	558.57(10)	1067.42(12)
Z	1	2	4
Reflections collected	3487	7821	14566
Independent reflections	76	1364	2438
R_{int}	0.0178	0.0186	0.0191
Data/restraints/parameters	76/6/12	1364/121/113	2438/1/146
Goodness-of-fit on F^2	3.645	1.033	1.080
R [$F^2 > 2\sigma(F^2)$]	0.1442	0.0567	0.0246
$wR(F^2)$ (all data)	0.4391	0.1630	0.0695
Flack parameter	-	0.06(2)	0.01(2)

2.3. Plasticity and Fabrication of Bulk Polycrystalline Films

Crystal **1** exhibited significant plasticity and malleability in the HTP, which allowed the fabrication of transparent polycrystalline films by hot pressing the powders **(Figure 3)**. Polycrystalline films with similar transparency can be obtained by pressing the powder at room temperature; however, they tend to have cracks, and are more fragile and difficult to handle than those obtained by hot pressing. This is attributable to the reduced plasticity and malleability of the crystals in the RTP. We measured the dielectric properties of crystal **1** using bulk polycrystalline films obtained by hot pressing.

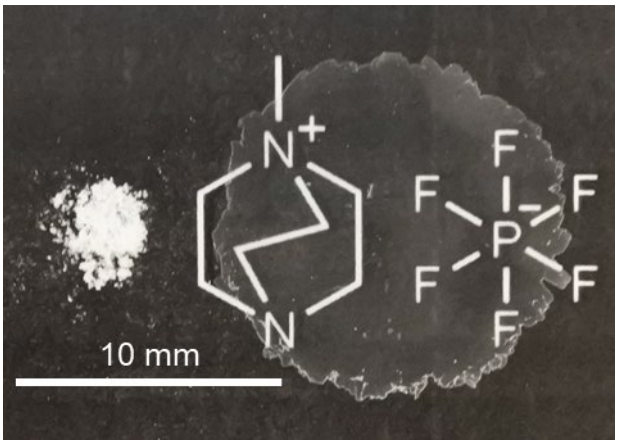

Figure 3. Photograph of powder and transparent polycrystalline film (thickness: 25 μm) of [MDABCO][PF_6] (**1**).

2.4. Dielectric Properties

The dielectric constants of crystal **1** were measured using a polycrystalline film with a thickness of 82 μm **(Figure 4)**. In addition to a small dielectric anomaly around 250 K, an abrupt change was observed at approximately 325 K, which corresponds to the two solid-solid phase transitions (LTP/RTP and RTP/HTP) of crystal **1**. The small ε' value (~35) at the RTP/HTP transitions indicates that the transition can be categorized into improper ferroelectric transitions, where the transitions are driven by the ordering of physical quantities that are different from the polarization, and the ε' value does not obey the Curie-Weiss law.[11] The phase transitions of crystal **1** can be interpreted based on the changes in the orientational order of the rotating molecules, whether they involve changes in the polarization of the crystal or not.

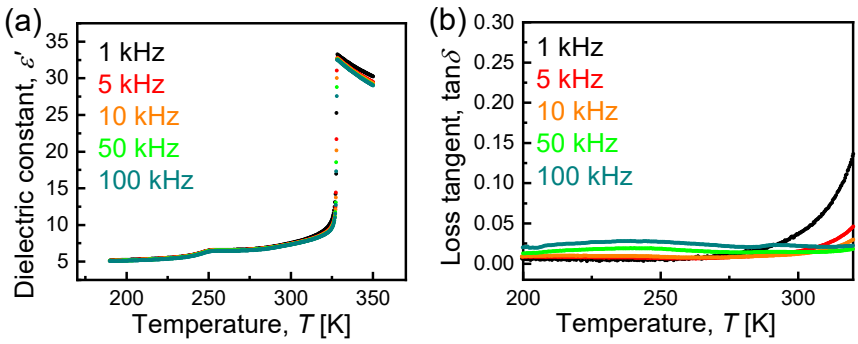

Figure 4. (a) Dielectric constant, ε', and (b) loss tangent, tanδ, of a polycrystalline film of [MDABCO][PF_6] (**1**) measured as a function of temperature at various frequencies.

2.5. Ferroelectric Properties of Bulk Polycrystalline Films

Bulk polycrystalline films of **1** exhibited ferroelectric performance at room temperature. A polarization-electric field (*P*–*E*) diagram measured at 300 K exhibited a well-defined rectangular hysteresis loop that indicated the ferroelectricity of **1** in the RTP **(Figure 5)**. The ferroelectric performance in the bulk polycrystalline film is consistent with the multiaxial ferroelectricity of the plastic/ferroelectric crystal **1**. The remanent polarization (P_r) and E_c values evaluated based on the intercepts in the *P*–*E* hysteresis loop were 3.5 μC cm^{-2} and 140 kV cm^{-1}, respectively. The P_r value was within the typical range of bulk samples of other plastic/ferroelectric crystals (approximately 4 μC cm^{-2})[5] and was comparable to that of a typical molecular ferroelectric crystal, triglycine sulfate (TGS, 2.8 μC cm^{-2}) in single crystals.[12] The large E_c value is attributable to the protruding shape of the [MDABCO]$^+$ cation and resulting distortion of the molecular arrangement in the RTP. The large E_c values were in sharp contrast to the small values, typically less than 5 kV cm^{-1}, observed for plastic/ferroelectric crystals of nearly spherical cations with pseudo-cubic rhombohedral lattices ($\alpha \approx 90°$).[6,8] The high processability of polycrystals due to malleability in the plastic crystal phase enabled the preparation of thin films of bulk polycrystals that were subjected to polarization switching of the ferroelectrics with large E_c values. In addition, the polycrystalline films of **1** showed moderate fatigue resistance. The P_r values did not decrease significantly after 10^4 cycles of polarization switching, while the E_c values and the contribution of conductivity increased slightly **(Figure S2)**. It was also observed that polarization switching occurs on a millisecond time scale under square-wave electric field pulses **(Figure S3)**.

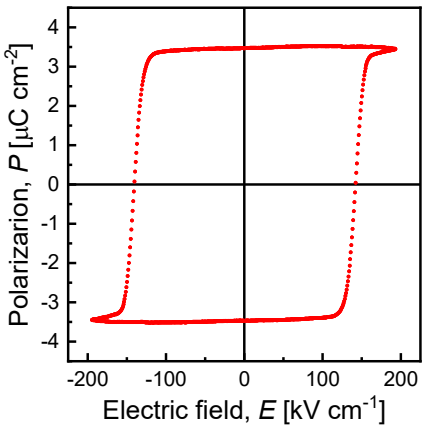

Figure 5. *P*–*E* hysteresis loop of a polycrystalline film (thickness: 14 μm) of [MDABCO][PF_6] (**1**) measured under a triangular-wave electric field of 50 Hz at 300 K.

2.6. Ferroelectricity in the LTP

The ferroelectricity of crystal **1** in the LTP was demonstrated by *P*–*E* hysteresis measurements using a thin crystalline film. The E_c values of bulk polycrystalline films of **1** significantly increased as the temperature decreased, and ferroelectric polarization switching required the application of larger electric fields to the films. In the LTP, the polycrystalline samples dielectrically broke down by the application of large electric fields before yielding *P*–*E* hysteresis loops. To achieve ferroelectric switching and to prove the ferroelectricity in the LTP, crystalline thin films were grown on an indium tin oxide (ITO)-coated glass substrate by drop casting an aqueous solution of **1**. This technique is widely used in the investigation of multiaxial molecular ferroelectric crystals.[13] The thin film obtained (thickness: 1.8 μm) was an aggregate of single crystals without domain walls and grain boundaries in the thickness direction. Well-defined rectangular hysteresis loops were obtained for a quasi-single-crystal thin film of **1**, which proved that the LTP, as well as the RTP, is a ferroelectric phase **(Figure 6)**. Although the *P*r values did not show significant changes between the two phases, the coercive voltage in the LTP (140 V) was considerably larger than that in the RTP (25 V).

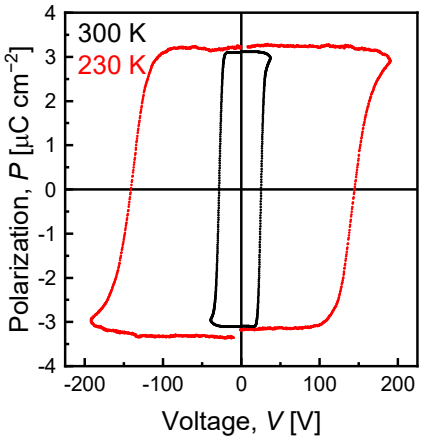

Figure 6. *P*–*E* hysteresis loops of thin crystalline film of [MDABCO][PF_6] (**1**) grown on a glass substrate with ITO electrode. The loops were measured under a triangular-wave electric field using a pulse train of positive up negative down (PUND) in the rate corresponding to 50 Hz cycle (pulse duration: 10 ms).[14]

2.7. Lattice Reorientation Induced by Electric Fields

The multiaxial ferroelectricity of crystal **1** was confirmed by powder XRD measurements of polycrystalline films. In multiaxial ferroelectric crystals, the polarization axis of the crystal in the ferroelectric phase can be changed into several different orientations depending on the direction of the applied electric field. The possible orientations are approximately equivalent to the polarization axis and are equivalent in the paraelectric crystal, which has a higher symmetry. In crystal **1**, for example, the ferroelectric phase belongs to the orthorhombic crystal system (point group: *mm*2), whereas the paraelectric phase belongs to the cubic crystal system (point group: $m\bar{3}m$). Thus, the polarization axis (*c*-axis) in the ferroelectric crystal can be changed into six different orientations that are equivalent face diagonals of the cubic crystal lattice in the paraelectric phase. The application of electric fields to the polycrystalline film changes the orientation of the crystal lattice of each polycrystal such that the polarization axis becomes as parallel as possible to the electric field direction and perpendicular to the film **(Figure 7)**. In contrast, in uniaxial ferroelectric crystals, the application of electric fields can only induce a 180º-flipping of the polarization and elimination of domain walls without changing the

orientation of the crystal lattice. The different behaviors of the multiaxial and uniaxial ferroelectric crystals can be distinguished by measuring the powder XRD patterns of the polycrystalline films before and after the application of electric fields. Although changes in the relative intensities of the reflections are expected for multiaxial ferroelectric crystals, the poling of uniaxial ferroelectrics does not cause significant changes in the diffraction pattern.

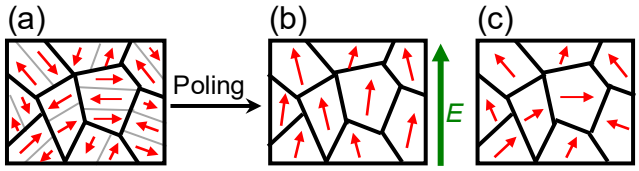

Figure 7. Schematic representation of reorientation of polarization axes (red arrows) and crystal lattices by application of electric fields. Crystal grains are enclosed by solid lines. (a) Before poling. The thin gray lines represent the domain walls in the crystal grains. (b) After poling expected for multiaxial ferroelectric crystals. Among several possible directions, the direction of the polarization of each crystal grain switched to the one that is most parallel to the applied electric field, which involves lattice reorientations. (c) After poling expected for uniaxial ferroelectric crystals. Of the two possible directions, the polarization of each grain was changed to the one more parallel to the applied electric field, which does not involve lattice reorientations.

Powder XRD measurements confirmed the multiaxial ferroelectricity of crystal **1**. **Figure 8** shows the XRD patterns of a polycrystalline film (thickness: 23 μm) measured at room temperature, before and after poling, and the pattern simulated from the crystal structure at 300 K.[15] The pattern of the film exhibited some degree of preferred orientation and did not show 012 and 021 reflections. Similar preferred orientations were observed for films of other plastic/ferroelectric crystals, which were induced during the film formation process.[7] The electric-field-induced changes in the diffraction patterns can be explained in terms of the lattice reorientation of each polycrystal in the film. The observed reflections can be classified into

three groups, and all their changes are consistent with the realignment of the polarization axes induced by the application of electric fields, as follows:

(i) The 102 and 120 reflections (2θ: 23 – 24°) correspond to the 111 reflection in the cubic crystal and are interchangeable by lattice reorientation. By applying electric fields perpendicular to the film, the 120 reflection disappeared, and the 102 reflection increased in intensity. These results indicate that crystalline grains in the film whose {120} planes are parallel to the film faces changed their lattice orientation, and the original {120} planes became {102} planes in the new orientation. Through this reorientation, the polarization of the crystals, which is parallel to the *c*-axis, has a larger vector component along the electric fields, which is more favorable under the electric fields;

(ii) The 002, 111, and 020 reflections (2θ: 18 – 20°) correspond to the 110 reflection in the cubic crystal. Although only the peak of the well-overlapping 111 and 020 reflections was observed before poling, the 002 reflection significantly increased in intensity after the poling. This change is consistent with the lattice reorientation induced by the electric fields, because the crystals contributing to the 002 reflection have the most favorable orientation under the electric fields, where the *c*-axis is parallel to the electric field;

(iii) The 110 reflection (2θ: 16 – 17°) corresponds to the reflection with half-integer indices (*i.e.*, 1 1/2 1/2) in the cubic crystal. The peak disappeared after the application of the electric fields. This change is also consistent with the lattice reorientation. After the application of the electric fields, the {110} planes changed to {101} planes, and the polarization of the crystal had an increased vector component along the electric field direction. However, the 101 reflection does not meet the reflection conditions for the space group $Pmc2_1$ ($l = 2n$ for $h0l$ type reflections) and was not observed accordingly.

All the changes described above are consistent with the lattice reorientation in a manner favored under the applied electric fields, and thus provide a decisive proof of multiaxial

ferroelectricity of **1**. Although ferroelectric performance in bulk polycrystalline forms has been reported for several plastic/ferroelectric crystals, this is the first demonstration of lattice reorientation. Moreover, the large distortion of the molecular arrangement in the ferroelectric phase yielded clear splitting between reflections that are equivalent in the cubic crystal, which enabled the observation of the changes in their relative intensities induced by the lattice reorientation.

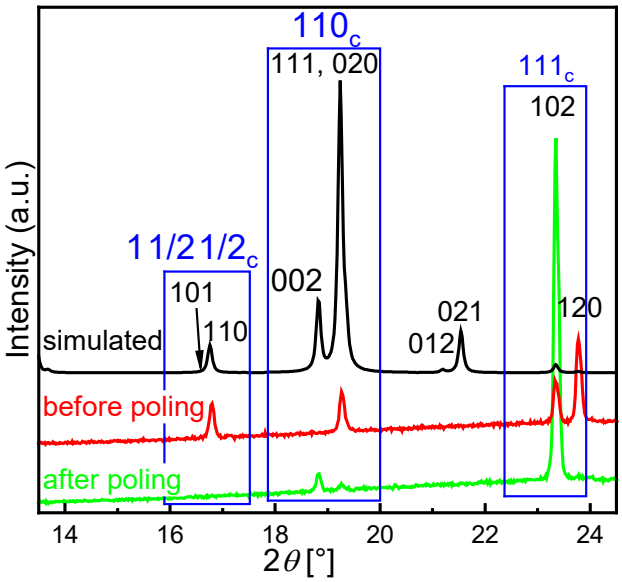

Figure 8. Powder XRD patterns of [MDABCO][PF_6] (**1**) at room temperature measured using Bragg-Brentano optical configuration.

3. Conclusion

In this study, we developed a new plastic/ferroelectric crystal [MDABCO][PF_6] (**1**). Owing to the cubic crystal structure in the plastic crystal phase, the crystal exhibits multiaxial ferroelectricity and ferroelectric performance in bulk polycrystalline films. Because of the protruding shape of the $[MDABCO]^+$ cation, the crystal in the ferroelectric phase shows a molecular arrangement largely distorted from a symmetric one in the cubic structure, to which the large E_c values are attributed. At the same time, the large distortion facilitates the observation of electric-field-induced lattice reorientation using powder XRD measurements.

Although a considerable number of plastic/ferroelectric crystals have been developed based on ionic molecules, the component ionic molecules have been mostly limited to those with nearly spherical shapes or with tetrahedral structures. The $[MDABCO]^+$ cation has been reported to form ferroelectric organic/inorganic hybrid perovskites consisting of three component ions,[16] but it has not been a constituent of two-component plastic/ferroelectric crystals. The $[PF_6]^-$ anion has also not been a constituent of plastic/ferroelectric crystals, which is in sharp contrast to the tetrahedral anions often found in ferroelectric crystals. This can be attributed to the centrosymmetric structure of the $[PF_6]^-$ anion, which is unfavorable for the formation of non-centrosymmetric ferroelectric crystals. In contrast, tetrahedral anions do not have a centrosymmetric structure, although they do have a highly symmetric globular structure. This study demonstrated that the combination of a protruding cation favoring asymmetric crystal structures and a highly symmetric anion favoring symmetric crystal structures can produce ionic molecular crystals with switchable crystal symmetry, that is, plastic/ferroelectric crystals. Having acquired new constituent members of plastic/ferroelectric crystals and expanding the range of target compounds with diverse characteristics, this study will accelerate the development of this new class of functional materials and facilitate their use in a variety of device applications.

4. Experimental Section

Synthesis: 1-methyl-4-aza-1-azoniabicyclo[2.2.2]octanium hexafluorophosphate ([MDABCO][PF_6]) (**1**) was obtained by ion exchange of 1-methyl-4-aza-1-azoniabicyclo[2.2.2]octanium iodide ([MDABCO][I]) (**2**). Compound **2** was prepared from DABCO and iodomethane according to the following procedure:[17] DABCO (0.912 g, 8.13 mmol) was dissolved in ethyl acetate (21 mL), which was cooled in an ice bath. Iodomethane (0.824 g, 5.81 mmol) was added dropwise to the solution, and a white precipitate formed immediately. Subsequently, the solution was stirred for 10 min at room temperature. The white precipitate was filtered off, washed once with cold ethyl acetate (5 mL), twice with cold hexane (5 mL × 2), and dried under

reduced pressure to give **2** (1.37 g, 5.39 mmol, 93%) as a white powder, which was purified by recrystallization from a propan-2-ol solution.

Compound **1** was obtained by ion exchange using an anion exchange resin (Wako DOWEX MONOSPHERE OH), followed by neutralization with hexafluorophosphoric acid. The white powder of **1** was obtained and purified by recrystallization from an aqueous propan-2-ol solution. Colorless single crystals suitable for single-crystal XRD analysis were obtained by the slow evaporation of water from an aqueous solution of **1** at room temperature. ^{1}H NMR (400 MHz, [D_6]DMSO, TMS): δ = 2.95 (s, 3H; CH_3), 3.01 (t, ^{3}J(H,H) = 7.5 Hz, 6H; $3CH_2$), 3.24 ppm (t, ^{3}J(H,H) = 7.5 Hz, 6H; $3CH_2$).

Sample Preparation: Bulk polycrystalline films of **1** were prepared by applying uniaxial pressure to the powders at 100 °C. For powder XRD measurements of lattice reorientation, the polarization of the polycrystalline film was confirmed by *P*–*E* hysteresis measurements, and the peripheral part of the sample that was not covered by the carbon electrodes was removed after the poling.

Thin-film crystals of **1** were grown by slow evaporation of an aqueous solution of **1** (0.88 wt%) on a glass plate with an ITO electrode. The glass plate was placed on a hot plate, whose temperature was set to 90 °C. The glass plate was ultrasonically cleaned sequentially in acetone, ethanol, deionized water, and ultrapure water prior to use.

Measurements: DSC measurements were performed under a flow of dry N_2 on a TA Instruments Discovery DSC250 using heating/cooling rates of 5 K min^{-1}. The phase-transition temperatures were determined using the tangent intersection method.

Powder XRD patterns were measured on a Bruker D8 ADVANCE ECO diffractometer (Ni-filtered Cu radiation) with a Bragg-Brentano optical configuration without sample rotation. The measured patterns of the samples used for the DSC and dielectric measurements confirmed the purity and identity of the phases, being compared with those simulated based on the crystal structures obtained from the single-crystal XRD analysis **(Figure S4)**. Variable-temperature

diffraction measurements were performed in a modular temperature chamber (Bruker, MTC-LOWTEMP).

Single-crystal XRD analyses were performed on a Bruker APEX II Ultra diffractometer (Mo Kα radiation, λ = 0.71073 Å). The temperature of the samples was controlled using a flow of N_2 and calibrated using a thermocouple. The crystal structures were solved by intrinsic phasing (SHELXT–2018)[18] and refined by full-matrix least-squares on F^2 using SHELXL–2018.[19] In the analysis of the crystal structure in the HTP, accurate molecular structures could not be obtained because of the completely disordered molecular orientations and the very weak diffraction in the high-diffraction angle region, and all atoms of the organic cation were refined as carbon atoms. Refinement details are provided in the Supporting Information as crystallographic information files embedding the SHELXL–2018 res files. CCDC 2130468−2130470 contains the supplementary crystallographic data for this paper. These data can be obtained free of charge from The Cambridge Crystallographic Data Centre via www.ccdc.cam.ac.uk/data_request/cif.

For the electrical measurements of bulk polycrystalline films, metal-insulator-metal capacitor structures were fabricated, where carbon paste was applied to both faces of the films to form electrodes. A homemade cryostat was used to control the temperature of the samples (190–350 K) under a helium atmosphere. The dielectric constant was measured using an Agilent E4980A precision LCR meter (1 kHz–100 kHz). The *P–E* diagrams and transient current responses were measured using a ferroelectric evaluation system (Toyo, FCE-3) with triangular- and square-wave electric fields, respectively. For the *P–E* diagram measurements of thin crystal films grown on ITO-coated glass substrates, a gallium-indium eutectic alloy was applied to the crystalline film to form the top electrode. The film thickness was estimated using atomic force microscopy (SII Nanotechnology, Nanocute) by measuring the depth of the gap formed in the film near the electrode.

Supporting Information

Supporting Information is available from the Wiley Online Library or from the author.

Acknowledgements
This work was supported by JSPS KAKENHI Grant Numbers JP18K19049 and JP19H00884.

Received: ((will be filled in by the editorial staff))
Revised: ((will be filled in by the editorial staff))
Published online: ((will be filled in by the editorial staff))

References

[1] S. Das, A. Mondal, C. M. Reddy, *Chem. Soc. Rev.* **2020**, 49, 8878.

[2] a) J. Timmermans, *J. Phys. Chem. Solids* **1961**, 18, 1; b) J. N. Sherwood, *The Plastically crystalline state: orientationally disordered crystals*, Wiley, Chichester; New York **1979**.

[3] a) D. R. MacFarlane, M. Forsyth, *Adv. Mater.* **2001**, 13, 957; b) J. M. Pringle, P. C. Howlett, D. R. MacFarlane, M. Forsyth, *J. Mater. Chem.* **2010**, 20, 2056; c) H. Zhu, D. R. MacFarlane, J. M. Pringle, M. Forsyth, *Trends Chem.* **2019**, 1, 126.

[4] a) B. Li, Y. Kawakita, S. Ohira-Kawamura, T. Sugahara, H. Wang, J. Wang, Y. Chen, S. I. Kawaguchi, S. Kawaguchi, K. Ohara, K. Li, D. Yu, R. Mole, T. Hattori, T. Kikuchi, S.-i. Yano, Z. Zhang, Z. Zhang, W. Ren, S. Lin, O. Sakata, K. Nakajima, Z. Zhang, *Nature* **2019**, 567, 506; b) P. Lloveras, A. Aznar, M. Barrio, P. Negrier, C. Popescu, A. Planes, L. Mañosa, E. Stern-Taulats, A. Avramenko, N. D. Mathur, X. Moya, J. L. Tamarit, *Nat. Commun.* **2019**, 10, 1803; c) A. Aznar, P. Lloveras, M. Barrio, P. Negrier, A. Planes, L. Mañosa, N. D. Mathur, X. Moya, J.-L. Tamarit, *J. Mater. Chem. A* **2020**, 8, 639; d) X. Moya, N. D. Mathur, *Science* **2020**, 370, 797; e) A. Aznar, P. Negrier, A. Planes, L. Mañosa, E. Stern-Taulats, X. Moya, M. Barrio, J.-L. Tamarit, P. Lloveras, *Appl. Mater. Today* **2021**, 23, 101023.

[5] J. Harada, *APL Mater.* **2021**, 9, 020901.

[6] J. Harada, T. Shimojo, H. Oyamaguchi, H. Hasegawa, Y. Takahashi, K. Satomi, Y. Suzuki, J. Kawamata, T. Inabe, *Nat. Chem.* **2016**, 8, 946.

[7] J. Harada, N. Yoneyama, S. Yokokura, Y. Takahashi, A. Miura, N. Kitamura, T. Inabe, *J. Am. Chem. Soc.* **2018**, 140, 346.

[8] J. Harada, Y. Kawamura, Y. Takahashi, Y. Uemura, T. Hasegawa, H. Taniguchi, K. Maruyama, *J. Am. Chem. Soc.* **2019**, 141, 9349.

[9] a) Y.-Y. Tang, W.-Y. Zhang, P.-F. Li, H.-Y. Ye, Y.-M. You, R.-G. Xiong, *J. Am. Chem. Soc.* **2016**, 138, 15784; b) Q. Pan, Z.-B. Liu, H.-Y. Zhang, W.-Y. Zhang, Y.-Y. Tang, Y.-M. You, P.-F. Li, W.-Q. Liao, P.-P. Shi, R.-W. Ma, R.-Y. Wei, R.-G. Xiong, *Adv. Mater.* **2017**, 29, 1700831; c) D. Li, X.-M. Zhao, H.-X. Zhao, X.-W. Dong, L.-S. Long, L.-S. Zheng, *Adv. Mater.* **2018**, 30, 1803716; d) Y. Xie, Y. Ai, Y.-L. Zeng, W.-H. He, X.-Q. Huang, D.-W. Fu, J.-X. Gao, X.-G. Chen, Y.-Y. Tang, *J. Am. Chem. Soc.* **2020**, 142, 12486; e) D. Li, X.-M. Zhao, H.-X. Zhao, Y.-P. Ren, L.-S. Long, L.-S. Zheng, *Phys. Status Solidi RRL* **2020**, 14, 1900644.

[10] a) A. Katrusiak, M. Szafrański, *Phys. Rev. Lett.* **1999**, 82, 576; b) M. Szafrański, A. Katrusiak, G. J. McIntyre, *Phys. Rev. Lett.* **2002**, 89, 215507; c) P.-P. Shi, Y.-Y. Tang, P.-F. Li, H.-Y. Ye, R.-G. Xiong, *J. Am. Chem. Soc.* **2017**, 139, 1319; d) Y.-Y. Tang, P.-F. Li, W.-Y. Zhang, H.-Y. Ye, Y.-M. You, R.-G. Xiong, *J. Am. Chem. Soc.* **2017**, 139, 13903.

[11] V. Dvořák, *Ferroelectrics* **1974**, 7, 1.

[12] M. E. Lines, A. M. Glass, *Principles and applications of ferroelectrics and related materials*, Clarendon press, Oxford **1977**.

[13] Y.-Y. Tang, P.-F. Li, W.-Q. Liao, P.-P. Shi, Y.-M. You, R.-G. Xiong, *J. Am. Chem. Soc.* **2018**, 140, 8051.

[14] M. Fukunaga, Y. Noda, *J. Phys. Soc. Jpn.* **2008**, 77, 064706.

[15] The strong 002 reflection at $2\theta = 26.6°$ due to carbon paste (graphite) appears outside the region shown in Figure 8.

[16] a) W.-Y. Zhang, Y.-Y. Tang, P.-F. Li, P.-P. Shi, W.-Q. Liao, D.-W. Fu, H.-Y. Ye, Y. Zhang, R.-G. Xiong, *J. Am. Chem. Soc.* **2017**, 139, 10897; b) H.-Y. Ye, Y.-Y. Tang, P.-F. Li, W.-Q. Liao, J.-X. Gao, X.-N. Hua, H. Cai, P.-P. Shi, Y.-M. You, R.-G. Xiong, *Science* **2018**, 361, 151.

[17] J.-Y. Kazock, M. Taggougui, B. Carré, P. Willmann, D. Lemordant, *Synthesis* **2007**, 2007, 3776.

[18] G. M. Sheldrick, *Acta Crystallogr., Sect. A* **2015**, 71, 3.

[19] G. M. Sheldrick, *Acta Crystallogr., Sect. C* **2015**, 71, 3.

Plastic/ferroelectric crystals have been developed using ionic molecules. Owing to the malleability in the plastic crystal phase, transparent polycrystalline films are readily available by pressing the powder at high temperatures. The obtained films show ferroelectricity at room temperature, and polarization switching proceeds through lattice reorientation of the crystals in the films.

Jun Harada,* Mika Takehisa, Yuto Kawamura, Haruka Takahashi, and Yukihiro Takahashi

Plastic/Ferroelectric Crystals with Distorted Molecular Arrangement: Ferroelectricity in Bulk Polycrystalline Films through Lattice Reorientation

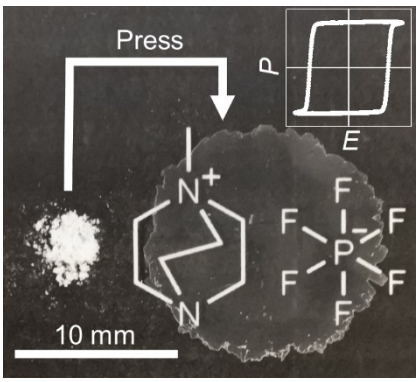

Supporting Information

Plastic/Ferroelectric Crystals with Distorted Molecular Arrangement: Ferroelectricity in Bulk Polycrystalline Films through Lattice Reorientation

Jun Harada, Mika Takehisa, Yuto Kawamura, Haruka Takahashi, and Yukihiro Takahashi*

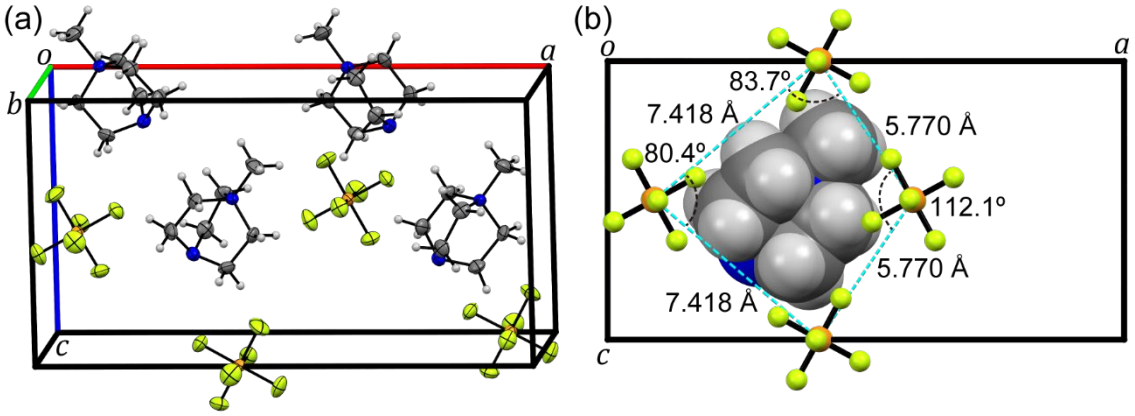

Figure S1. (a) Crystal structure of [MDABCO][PF_6] (**1**) at 180 K (LTP) with thermal ellipsoids drawn at 50% probability. (b) Projection along the *b*-axis, where the distorted CsCl-type arrangement is outline by dashed cyan lines connecting phosphor atoms of the $[PF_6]^-$ anions.

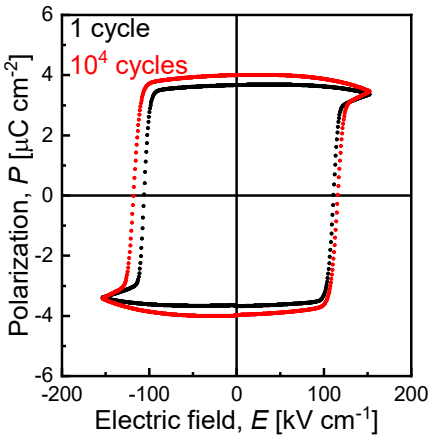

Figure S2. *P*–*E* hysteresis loops of a polycrystalline film (thickness: 19 μm) of [MDABCO][PF_6] (**1**) measured under a triangular-wave electric field of 10 Hz at 300 K. After the measurement of the black loop, 10^4 cycles of the electric field were applied to the sample, before the red loop was recorded.

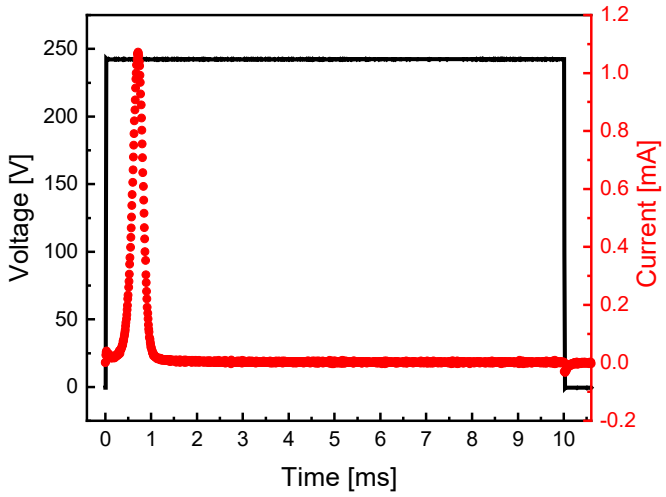

Figure S3. A 10-ms electric field pulse input (black) and the transient current response (red) of ferroelectric switching measured using a polycrystalline film (thickness: 19 μm) of [MDABCO][PF_6] (**1**) at 300 K.

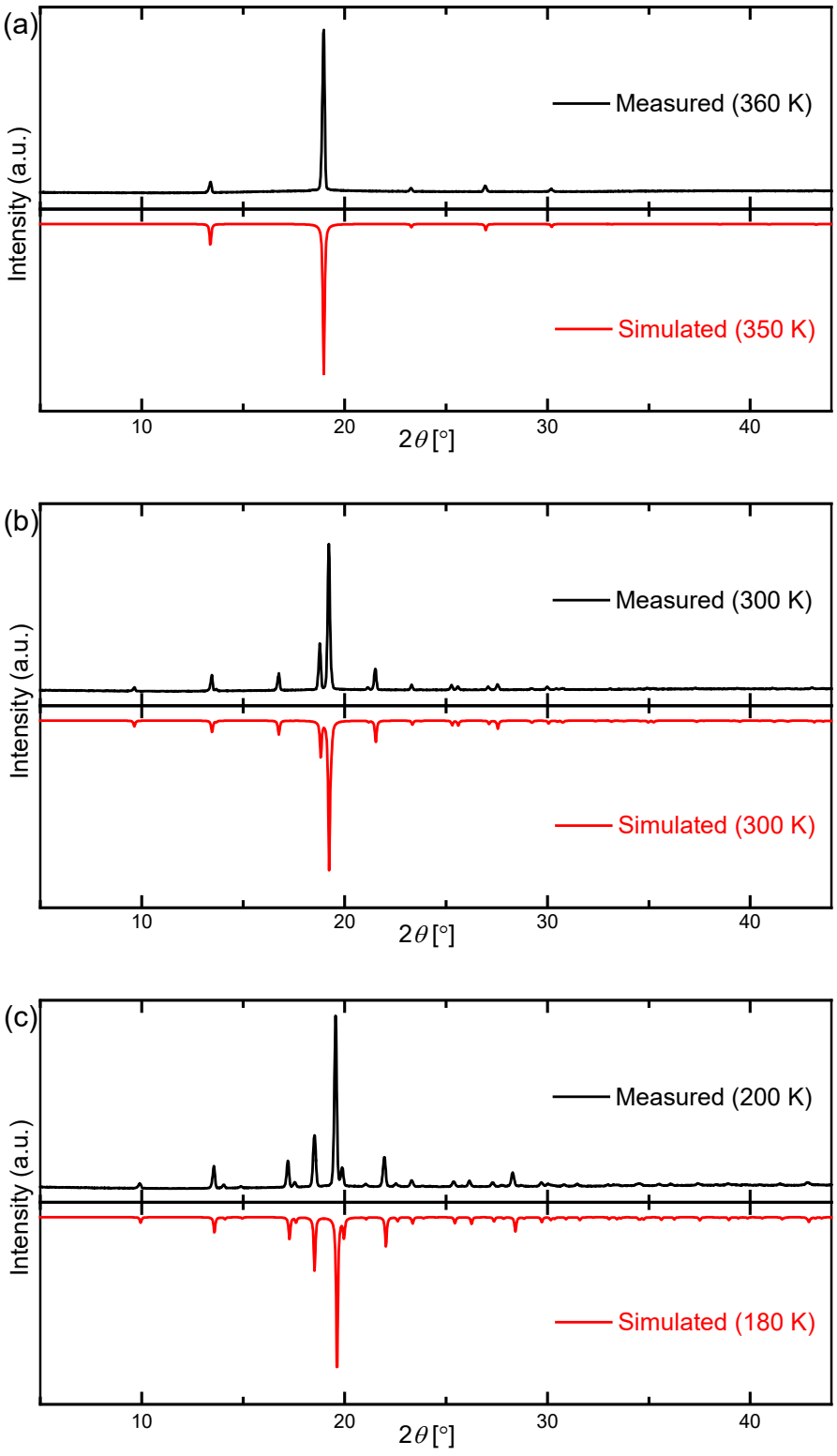

Figure S4. Experimental and simulated powder XRD patterns of [MDABCO][PF_6] (**1**) in (a) HTP, (b) RTP, and (c) LTP.